Heliyon 10 (2024) e40774

Contents lists available at ScienceDirect

Heliyon

journal homepage: www.cell.com/heliyon

Research article

Design and in silico analysis of a novel peptide-based multiepitope vaccine against glioblastoma multiforme by targeting tumor-associated macrophage

Reza Salahlou [a,b,e], Safar Farajnia [b,c,*], Effat Alizadeh [a], Siavoush Dastmalchi [b,d,f], Nasrin Bargahi [b], Leila Rahbarnia [g], Safooreh Hoseinpour Steyar [c]

[a] Department of Medical Biotechnology, Faculty of Advanced Medical Sciences, Tabriz University of Medical Sciences, Tabriz, Iran
[b] Biotechnology Research Center, Tabriz University of Medical Sciences, Tabriz, Iran
[c] Drug Applied Research Center, Tabriz University of Medical Sciences, Tabriz, Iran
[d] Department of Medicinal Chemistry, School of Pharmacy, Tabriz University of Medical Sciences, Tabriz, Iran
[e] Student Research Committee, Tabriz University of Medical Sciences, Tabriz, Iran
[f] Faculty of Pharmacy, Near East University, P.O. Box 99138, Nicosia, North Cyprus, Mersin 10, Turkey
[g] Infectious and Tropical Diseases Research Center, Tabriz University of Medical Sciences, Tabriz, Iran

ARTICLE INFO

Keywords:
Glioblastoma cancer
Tumor-associated macrophages
CD204
Immunotherapy
Molecular docking
Molecular dynamics (MD) simulation

ABSTRACT

CD204 is a distinct indicator for tumor-associated macrophages (TAMs) in glioma. Evidence indicates that CD204-positive TAMs are involved in the aggressive behavior of various types of cancers. This study was conducted to develop a new and effective peptide-based vaccine for GBM, specifically targeting CD204. Epitopes of the target protein were identified using NetMHCpan 4.1a, NetMHCIIpan-4.0, and ABCpred tools. Subsequently, the predicted epitopes were evaluated using bioinformatics tools to assess their antigenicity, non-allergenicity, immunogenicity, non-toxicity, and potential to stimulate the production of IL-4 and IFN-γ in HTL epitopes. Selected T-cell epitopes demonstrated a robust binding affinity with the particular HLA alleles. Finally, four HTL epitopes, three CTL epitopes, and two B-cell epitopes, jointed via linkers and adjuvant, were used for the final vaccine construct design. Analysis disclosed that the developed vaccine demonstrated robust antigenic properties while proving soluble, stable, non-toxic, and non-allergenic. Additionally, molecular docking studies and molecular dynamics simulations confirmed a robust correlation between the designed vaccine and TLR-2 and TLR-4 immune receptors. The molecular docking results demonstrated a strong interaction between the newly developed vaccine and TLR2 (−895.1 kcal/mol) and TLR4 (−881.0 kcal/mol) receptors. During the simulation, the vaccine-TLR2 and vaccine-TLR4 complexes exhibited binding energies of −113.41 and −106.61 kcal/mol, respectively. Analysis by different bioinformatic tools indicated the potential of the designed vaccine in immune stimulation and a significant elevation in IgG and IgM antibodies, T-helper cells, T-cytotoxic cells, INF-γ, IL-2, and IL-4. Research findings show that the newly designed multi-epitope vaccine is promising in providing long-term immunity against GBM and offers a promising therapeutic alternative.

* Corresponding author. Biotechnology Research Center, Tabriz University of Medical Sciences, Tabriz, Iran.
E-mail address: farajnia@gmail.com (S. Farajnia).

https://doi.org/10.1016/j.heliyon.2024.e40774
Received 18 August 2024; Received in revised form 23 November 2024; Accepted 27 November 2024
Available online 28 November 2024

1. Introduction

Glioblastoma multiforme (GBM) is recognized as the most malignant and aggressive variant of glioma and continues to be a prominent contributor to mortality rates in the realm of human cancers [1]. Given the unsatisfactory results observed following conventional treatment methods, there exists an urgent requirement for novel therapeutic strategies. Much evidence suggests that the tumor microenvironment facilitates glioma progression. It comprises stromal cells and a variety of immune cells, such as fibroblasts, regulatory T cells (Tregs), endothelial cells, dendritic cells (DCs), tumor-infiltrating lymphocytes (TILs), myeloid-derived suppressor cells (MDSCs), natural killer (NK) cells, tumor-associated macrophages (TAMs) [2]. Among these, it is believed that TAMs exert a significant influence and contribute to approximately 30 % of the total mass of the tumor [3]. They comprise three distinct subpopulations based on the origin of the cells, specifically extra-parenchymal macrophages, brain-resident microglia, and bone marrow-derived macrophages (BMDMs) [4]. In contrast to traditional M1-activated macrophages, known for enhancing the antitumor immune response, TAMs exert an immunosuppressive function and are therefore classified as an alternatively activated M2 phenotype [5,6]. By secreting VEGF, IL-6, TGFβ1, PDGF, MMP2, periostin, and MMP9, TAMs facilitate glioma progression by maintaining the glioma stem cell phenotype, stimulating angiogenesis, and controlling extracellular matrix (ECM) degradation. Consequently, this complex interplay leads to the growth and invasion of glioma and the establishment of distant pre-metastatic niches [7,8]. Additionally, the systemic immune response is suppressed by the immunosuppressive microenvironment created by TAMs, which also increases T-cell apoptosis, inhibits the response of cytotoxic T lymphocytes (CTLs), and leads to growth encouragement in other immunosuppressive cells like Tregs and MDSCs [9,10]. Considering the primary role of TAMs in stimulating glioma cancer progression, specifically targeting TAMs strategically can yield effective results in halting the advancement of this malignancy. CD204, also called macrophage scavenger receptor 1 (MSR1), is widely acknowledged as a particular marker of TAM within glioma [11]. Many metabolic processes in macrophages are regulated by CD204, including reactive oxygen species production, phagocytosis, adhesion, and immunity [12]. Furthermore, TAMs expressing CD204 reduce T cell activation via down-regulation of toll-like receptor 4 signaling [6]. The expression of CD204 in TAMs in the glioma microenvironment is linked to the histological level and prognosis of glioma. CD204 plays a crucial role in glioblastoma due to its expression on M2-polarized tumor-associated macrophages. These TAMs promote tumor growth and suppress immune responses, creating an immunosuppressive environment that aids tumor progression. Advantages of targeting CD204 over other markers include its specific role in TAMs and glioma, making it a more promising target compared to others: A) Prominent Expression: CD204 is highly expressed in glioblastoma tumors, making it a readily identifiable target. B) Immunosuppressive Role: By targeting CD204, it's possible to disrupt the immunosuppressive environment created by M2-polarized TAMs, potentially enhancing the efficacy of immunotherapies. C) Prognostic Value: High expression of CD204 has been associated with poor prognosis, indicating its significant role in tumor progression. D) Therapeutic Potential: Blocking CD204 can prevent the immunomodulatory mechanisms of TAMs, allowing for better immune cell infiltration and tumor control [13,14]. These observations suggest immunotherapy targeting CD204 may be a viable treatment option for gliomas [15]. Upon the migration of tumor antigens into the organism in various modalities, they undergo phagocytosis, and intracellular expression, and are proficiently processed by specialized antigen-presenting cells (APCs). The major histocompatibility complex (MHC) associated with dendritic cells facilitates the presentation of antigens on their surface. These MHC complexes subsequently engage in the activation of antigen-specific T-cells through their interaction with T-cell receptors (TCR) located on the surface of T-cells, thereby contributing to the precise, sustained, and safe eradication of tumor cells while simultaneously impeding tumor proliferation [16]. Currently, multi-epitope peptide cancer vaccines have surfaced as a hopeful strategy for the next generation of cancer treatments. These vaccines either with augmentation of the reactions of CTLs and helper T lymphocytes (HTLs) or with inhibition of the immune response suppressors stimulated immune responses against tumor cells. There exists the potential for an acceleration of the anti-tumor immunity activity. Hence, it becomes crucial to develop an innovative therapeutic cancer vaccine capable of inducing both cellular and humoral immune responses [17]. One of the primary drawbacks associated with multi-epitope vaccines resides in their limited immunogenicity, as the presence of proteinases within the body can rapidly degrade the antigenic peptides, rendering them difficult for immune cell receptors to react. To boost the immune response elicited by multi-epitope vaccines, one proposed strategy involves the utilization of adjuvants in the vaccine design. Epithelial cells produce short, positively charged antimicrobial peptides known as human beta-defensins (HBDs). These compounds have antibacterial and immunomodulatory properties contributing to adaptive and innate immunity [18]. The advancement of cancer vaccine development is fraught with numerous challenges and limitations, which can obstruct the timely and efficient responses to cancer therapies. A) Antigen Degradation: One significant hurdle is antigen degradation. The efficacy of the vaccination may be diminished if the proteins utilized as antigens degrade before being recognized by the immune system. Bioinspired nano-vaccines, constructed through antigen pre-degradation, offer a promising method for personalized cancer immunotherapy, utilizing advanced biomaterials and nanotechnology to enhance neoantigen delivery and immune response [19]. B) Immune Evasion: Several strategies are used by cancer cells to evade the immune system, which makes vaccinations less effective. Developing adjuvants to boost immune responses and combining vaccinations with other treatment modalities are two ways to combat this immune evasion [20]. C) Tumor Heterogeneity: Tumor heterogeneity significantly complicates the development of effective cancer vaccines, as the variable antigen expression among tumor cells can hinder the overall efficacy of a single-vaccine approach. Personalized vaccines targeting patient-specific antigens are under investigation as a potential solution to this challenge [21]. Regarding the novelty of the work, to the best of our knowledge, this is the first report of the development of a peptide-based vaccine targeting CD204 protein in GBM. About the approach used in our study, it should be noted that subunit cancer vaccines, incorporating specific antigens, have demonstrated the capability to elicit protective immune responses, potentially aiding in both the prevention and elimination of cancer. Peptide-based cancer vaccines have emerged as a favored treatment strategy in recent years, commonly integrated with alternative cancer therapeutic approaches. Numerous clinical studies have investigated the safety and effectiveness of peptide-based cancer

vaccines, yielding encouraging results. Developments in technologies like next-generation sequencing, whole-exome sequencing, and in silico strategies have advanced the identification of antigens, thus making it increasingly practical [22–26].

The CD204 antigen was analyzed in the present investigation to determine the existence of CTL, HTL, and Interferon-gamma (IFN-γ) epitopes by utilizing diverse immunoinformatics tools. The epitopes that were acquired underwent a characterization process, and those that demonstrated immunogenic, antigenic, non-allergenic, and non-toxic properties were utilized to create the vaccine. Then, immunoinformatics tools were used to examine the mechanism of vaccine binding with immune receptors, its effect on the immune system, and its potential for large-scale production. This investigation not only provides theoretical guidance and empirical evidence for forthcoming studies on CD204 immunization, but it also represents novel concepts for the advancement of immunizations targeting alternative TAMs.

2. Materials and methods

2.1. Protein and adjuvant sequence retrieval

We employed the UniProt database to obtain the FASTA-formatted amino acid sequences of both the target protein, CD204 (Accession No. P21757), and the adjuvant, Beta-defensin 3 (Accession No. Q5U7J2).

2.2. Identification of cytotoxic and helper T lymphocyte epitopes

NetMHCpan 4.1a tool (https://services.healthtech.dtu.dk/services/NetMHCpan-4.1a/), which utilizes artificial neural networks (ANNs) to determine peptides with affinity to all known sequences of MHC molecules, was exploited to find CTL epitopes, specifically targeting twelve prominent HLA supertypes (HLA-A02:01(A2), HLA-A01:01(A1), HLA-A03:01(A3), HLA-A26:01(A26), HLA-A24:02 (A24), HLA-B08:01(B8), HLA-B07:02(B7), HLA-B39:01(B39), HLA-B27:05 (B27), HLA-B40:01 (B40), HLA-B15:01(B15), HLA-B58:01 (B58)) for binding analysis [27]. In this research, epitope prediction was carried out using 9-mer peptides, considering that the MHC I protein's open-binding groove usually accommodates peptides ranging from 8 to 14 residues. Further, a threshold adjustment of 0.5 was made for strong binders, and a threshold adjustment of 2 was made for weak binders. Similarly, By using the ANN algorithm, the NetMHCIIpan-4.0 server (https://services.healthtech.dtu.dk/services/NetMHCIIpan-4.0/) was employed to identify HTL-specific epitopes involved in MHC-II alleles HLA-DR, HLA-DQ, and HLA-DP [28]. In this research, epitope prediction was conducted using peptides with a length of fifteen amino acids, with the thresholds for distinguishing weak and strong binders determined at 5 % and 1 %, respectively.

2.3. Identification and analysis of B-cell epitopes

B-cell epitopes play a crucial role in initiating antibody-mediated or humoral immune responses. The linear epitopes of B-cells were predicted via the ABCpred tool (https://webs.iiitd.edu.in/raghava/abcpred/ABC_submission.html). The chosen threshold for prediction involved establishing a threshold of 0.8 and a window length of 16 mers [29]. Also, discontinuous B-cell epitopes were determined using the IEDB interface utilizing the ElliPro tool (http://tools.iedb.org/ellipro/). This prediction was conducted using a 3D model of the vaccine structure with default parameters: a minimum residual score of 0.5 and a maximum distance of 6 [30]. Tornton's method and the residue clustering algorithm are utilized on this server. The ElliPro program assigns scores to an individual epitope based on an average of the protrusion index (PI) values across its residues. The majority of calculations are based on protein regions that protrude from the protein globule's surface. Protein regions extending from the globular surface are more prone to interact with antibodies. Hence, the PI score correlates directly with solvent accessibility, significantly influencing the function and structure of biological macromolecules.

2.4. Antigenicity, allergenicity, toxicity, and surface accessibility of predicted epitopes

The VaxiJen 2.0 program (https://www.ddg-pharmfac.net/vaxijen/VaxiJen/VaxiJen.html) was employed to check an individual epitope antigenicity. Subsequently, epitopes demonstrating an antigenicity value above 0.5 were subjected to allergenicity and toxicity examination by the AllergenFP v1.0 (https://ddg-pharmfac.net/AllergenFP/) [31] and ToxinPred (https://webs.iiitd.edu.in/raghava/toxinpred/design.php) [32] tools, respectively. AllergenFP v1.0 utilizes five E-descriptor-based fingerprinting to anticipate epitope allergenicity, achieving an accuracy rate of 88 %. Solvent accessibility of the engineered vaccine structure was further predicted using the NetSurfP-3.0 (https://services.healthtech.dtu.dk/services/NetSurfP-3.0/) computational platform. Using PyMOL v2.4 software surface mode, epitope accessibility was determined on protein surfaces.

2.5. Evaluation of CTL epitope immunogenicity and confirmation of HLA class I allele binding

Immunogenicity refers to an agent's ability to trigger an immunological response in the body, such as an antigen or epitope. The IEDB's Class I Immunogenicity Tool (http://tools.iedb.org/immunogenicity/) was employed to assess CTL immunogenicity, while the parameters were left as default. When the immunogenicity score is high, the host immune response is likely [33]. The TepiTool, accessed via http://tools.iedb.org/tepitool/, was employed within IEDB to confirm the binding of HLA class I alleles to CTL epitopes, utilizing a recommended algorithm. Epitopes scoring a percentile rank of ≤ 1 are typically considered to exhibit a robust binding

affinity to HLA class I molecules [34].

2.6. Screening of cytokine induction of HTL epitopes

The IFN-γ plays a major role in enhancing antigen presentation, leukocyte transport, and stimulating T-cell differentiation, as well as making antibacterial substances more effective [35]. Furthermore, interleukin-4 (IL-4) promotes the proliferation and differentiation of B and T cells [36]. Consequently, we utilized the IFN epitope (https://webs.iiitd.edu.in/raghava/ifnepitope/predict.php) and IL4Pred (https://webs.iiitd.edu.in/raghava/il4pred/pep_test.php) servers to estimate the potential of the identified HTL epitopes in inducing the secretion of IFN-γ and IL-4 [37,38].

2.7. Molecular docking between MHC molecules and T-cell epitopes

Molecular docking was carried out to examine the interactive patterns between MHC molecules and T-cell epitopes. The PEP-FOLD 3 (https://bioserv.rpbs.univ-paris-diderot.fr/services/PEP-FOLD3/) tool generated 3D models of selected T-cell epitopes [39]. The RCSB PDB tool (https://www.rcsb.org/) was the direct source for obtaining the 3D structures of MHC class I (HLA-A*02:01 PDB ID 7KGP, HLA-A*24:02 PDB ID 7MJA, HLA-B*07:02 PDB ID 6AT5) and MHC class II molecules (HLA-DP1 PDB ID 7T6I and HLA-DRB1 PDB ID 6BIN) [40]. The Swiss-Pdb Viewer software was subsequently employed to minimize energy for both the receptors and ligands [41]. Then, molecular docking between MHC molecules and T-cell epitopes was carried out using Autodock Vina within the PyRx v0.8 platform [42]. The docking results were visualized with PyMOL v2.4 software.

2.8. Vaccine construction

Multi-epitope peptide vaccines have low immunogenicity compared to traditional vaccines. To boost the immune response elicited by the vaccine candidate, the addition of β-defensin 3 at the N-terminus of the vaccine was implemented as an adjuvant. Furthermore, suitable connectors were introduced between the epitopes to inhibit the creation of novel epitope bonds and maintain the distinct immunogenicity of each epitope. Next, the adjuvant and vaccine were connected using the EAAAK linker. The HTL, B-cell, and CTL epitopes were also attached utilizing GPGPG, KK, and AAY linkers, respectively [43,44].

2.9. Assembly of the vaccine construct

The antigenicity of the vaccine candidate was initially forecasted using the VaxiJen2.0 server and subsequently validated through the ANTIGENpro program. The tool utilized to evaluate allergenicity was AllerTOP v.2.0 (https://www.ddg-pharmfac.net/AllerTOP/) [45], while the ToxinPred (https://webs.iiitd.edu.in/raghava/toxinpred/algo.php) tool was employed to evaluate toxicity [32]. Subsequently, the ProtParam program (https://web.expasy.org/protparam/) was utilized to examine the physicochemical characteristics of the proposed vaccine. This encompassed amino acid count, instability index, theoretical isoelectric point (PI), molecule weight, aliphatic index, half-life, and GRAVY [46]. The probability of obtaining soluble expression of the proposed vaccine in *E. coli* was estimated using the SOLpro tool (https://scratch.proteomics.ics.uci.edu/), yielding a precision of approximately 74 % [47]. In addition, the vaccine was tested for the prediction of potential transmembrane helices using the DeepTMHMM server and the identification of signal peptides using the SignalP6.0 server.

2.10. Prediction and validation of the secondary and 3D structure of the vaccine construct

The Prabi tool (https://npsa-prabi.ibcp.fr/cgi-bin/npsa_automat.pl?page=/NPSA/npsa_gor4.html) analysis workbench was utilized to perform the secondary structure prediction of the designed vaccine, determining the percentages of helices, strands, and coils. In this server, GOR IV is used for prediction, which has an accuracy of 64.4 % [48]. Additionally, the Robetta tool (https://robetta.bakerlab.org/) was utilized to anticipate the tertiary structure of the vaccine. The server uses comparative modeling when a matching pattern exists in the database; otherwise, it resorts to ab initio structure prediction [49]. The most accurate predicted model underwent validation utilizing the SAVES v6.0 program (https://saves.mbi.ucla.edu/). This server employs an array of tools, including PROCHECK for visualizing the Ramachandran plot, Verify 3D for assessing the compatibility of the atomic model (3D), and ERRAT for analyzing nonbonded atomic interactions. The ProSA program assesses the model's overall quality and detects possible errors [50].

2.11. Molecular docking of the toll-like receptors and vaccine

The molecular binding process involving the designed vaccine and its receptor can help clarify how these two molecules bind to each other. A transmembrane protein found in many different organs, particularly in macrophages and monocytes, is called toll-like receptor 4 (TLR4). By directly detecting pathogen-associated molecular patterns (PAMPs) for instance lipopolysaccharide (LPS), lipoteichoic acid (LTA), and double-stranded RNA (dsRNA), it has a pivotal function in the initiation of innate immunity [51]. TLR2, a member of the TLR family, regulates the function of natural killer (NK) cells, T cells, macrophages, dendritic cells (DC), and other immune cells [51,52]. Molecular docking experiments were executed using the Clus Pro 2.0 program (https://cluspro.org/help.php) to assess the interaction between the protein vaccine and TLR2 (PDB ID 6NIG) as well as TLR4 (PDB ID 4G8A). This server arranges the docking complexes into clusters based on their lowest and central energy values [53]. Next, the HADDOCK 2.4 program (https://

wenmr.science.uu.nl/haddock2.4/) received the desired docking model and default parameters for confirmation [54]. Moreover, the PDBsum tool (http://www.ebi.ac.uk/thornton-srv/databases/cgibin/pdbsum/GetPage.pl?pdbcode=index.html) was exploited to survey the amino acids implicated in the interaction between the TLRs and vaccine [55].

2.12. Molecular dynamic simulation

A molecular dynamics (MD) simulation was performed via Gromacs v2022.1 to confirm the atomic-level stability of the vaccine receptor complexes [56]. The root mean square deviation (RMSD), the radius of gyration (rGyr), root mean square fluctuation (RMSF), the number of hydrogen bonds, and the total solvent accessible surface area (SASA) were utilized to reflect the simulation results. The topology and coordinate file of the vaccine-receptor complex were produced in the initial phase by including the AMBER14SB_-PARMBSC1 force field [57]. The complex system was later hydrated by adding TIP3P water molecules with transferable intermolecular potential, and counter ions (Na+ and Cl-) were included to balance the system's charge. After that, energy reduction was carried out until the maximum force of ≤1000.0 kJ/mol/nm, or the appropriate threshold, was reached. To ensure uniform temperature and pressure throughout, simulations in both NPT and NVT ensembles were conducted, spanning 1ns and 200ps, respectively. Through this process, the system temperature was adjusted and stabilized at 310K, while the pressure was equilibrated to 1atm. The system's temperature was managed by the utilization of a modified Berendsen thermostat [58], while the pressure was stabilized using the Parinello-Rahman barostat [59]. Subsequently, an isothermal and isobaric system was simulated with MD for 50 ns. Finally, The LINCS algorithm was employed to enforce limitations on the hydrogen bond formation and dynamics [60], and the Long-range electrostatic interactions were computed employing Particle-Mesh Ewald summation [61]. Utilizing the gmx_MMPBSA v1.56 program, the final 10 ns of the trajectory were isolated to calculate the binding free energy between the TLRs and vaccine [62]. Furthermore, the gmx_MMPBSA v1.56 program was utilized to examine the energy contribution from all residues near the ligand and receptor, within a distance of 4 Å. In the current research, the MM-PBSA technique was utilized to forecast the binding free energy of the intricate system, the elucidation of which is expressed mathematically.

2.13. Immune response simulation

To evaluate the immunogenicity of the designed vaccine, in silico immune simulation was performed using the online simulation server C-ImmSim (https://kraken.iac.rm.cnr.it/C-IMMSIM/). This tool may simulate an immunological response similar to that of a lymphoid organ, bone marrow (containing lymph cells), and the mammalian thymus (containing T cells) [63]. By analyzing the simulation findings, we might be able to assess the vaccine immunogenicity and the potential immune response it could trigger. The related parameters with the administration dose and time of vaccination were changed based on previous research including 1000 units of vaccine per injection with four-week intervals between each injection, for a complete course of three injections [64]. The overall count of steps was determined to be 1050, distributed as follows: a 1-time step for the initial injection, 84 for the second, and 168 for the third. The human MHC molecule compositions included HLA-A*02:01, HLA-A*24:02, HLA-B*07:02, HLA-DRB1*07:01, and HLA-DRB1*04:04, while the remaining parameters remained unaltered.

2.14. Codon optimization and cloning

The Java Codon Adaptation (https://www.jcat.de/) Tool for the *E. coli* strain K12 prokaryotic expression system was utilized to improve the codon for the final vaccine protein [65]. We avoided prokaryotic rho-independent transcription terminators, ribosome binding sites, and host codon usages due to the differences in native and foreign gene expression. The quantification of protein expression level was determined by assessing the codon adaptation index (CAI) value and GC content of the adapted genetic sequence, which significantly influence protein synthesis efficiency. For the cloning of the refined gene sequence of the ultimate vaccine construct into the *E. coli* pET-30a (+) vector, we incorporated *Xho*I and *Eco*RI restriction sites at the C and N-terminals of the sequence,

Table 1
The selected CTL epitopes of CD204 and its immunogenic properties.

Epitope	Antigenicity	Immunogenicity	Allergenicity	Toxicity	NetCTLpan1.1 server	Tepitool server
AMKEEQVHL	0.7524	0.07295	Non allergen	Non-toxic	HLA-A*02:01, HLA-B*08:01, HLA-B*15:01	HLA-B*13:01, HLA-B*48:01, HLA-A*02:01, HLA-B*13:02, HLA-A*02:06, HLA-B*15:01, HLA-B*08:01, HLA-B*15:25, HLA-A*32:01, HLA-B*46:01, HLA-B*52:01, HLA-B*37:01, HLA-B*15:02
RFNDILLQL	1.5199	0.06234	Non allergen	Non-toxic	HLA-A*24:02	HLA-A*23:01, HLA-A*24:02, HLA-A*32:01, HLA-B*13:01, HLA-B*48:01, HLA-A*30:01, HLA-A*30:02, HLA-A*29:02, HLA-B*13:02, HLA-B*38:01, HLA-B*27:02, HLA-B*08:01, HLA-B*58:02, HLA-A*02:01, HLA-B*27:05, HLA-A*02:06
GPHEGRVEI	0.6667	0.28631	Non allergen	Non-toxic	HLA-B*07:02	HLA-B*07:02, HLA-B*55:01, HLA-B*56:01, HLA-B*35:03, HLA-B*51:01, HLA-B*39:01, HLA-B*14:02

respectively. Finally, the SnapGene software successfully integrated an enhanced genetic sequence into the pET-30a(+) plasmid, ensuring efficient production and expression of the vaccine.

3. Results

3.1. Screening of epitopes

HTL and CTL epitopes were identified for designing a novel epitope vaccine based on twelve major HLA-I supertypes and HLA-DQ, HLA-DR, and HLA-DP MHC-II alleles. Following the assessment of immunogenicity, antigenicity, allergenicity, and toxicity the potential to stimulate the production of IL-4 and IFN-γ (for HTL) were investigated. we pinpointed three optimal CTL epitopes from a pool of 46 epitopes (Table 1), four favorable HTL epitopes from a collection of 76 epitopes (Table 2), and two suitable B cell epitopes from a sum of 20 epitopes (Table 3), all intended for the formulation of a peptide-based vaccine. The solvent accessibility analysis of the vaccine construct indicated that the chosen epitopes were adequately exposed to the solvent (Fig. S1). Epitopes selected for further study were found to be on the protein's external surface, indicating their accessibility for interactions with other biological system molecules, and these locations were made visible through the utilization of PyMOL software version 2.4 (Fig. S2).

3.2. Molecular docking between MHC molecules and T cell epitopes

Molecular docking between T cell epitopes and MHC molecules was conducted using Autodock Vina. Based on the results, there was a range of binding affinities between MHC I alleles with CTL epitopes, for epitope AMKEEQVHL with allele HLA-A*02:01 a binding affinity of −9.5 kcal/mol was reported while epitope RFNDILLQL with allele HLA-A*24:02 indicated a binding affinity equal to −9.0 kcal/mol, and epitope GPHEGRVEI with binding affinity −10.3 kcal/mol banded to allele HLA-A*07:02. HLA-DRB1 was selected for QQEEISKLEERVYNV, HFQNFSMTTDQRFND, and NMEKRIQHILDMEAN epitopes with binding affinity −10.7, −8.3, and −9.5 kcal/mol, respectively, while HLA-DP1 was selected for the EERVYNVSAEIMAMK epitope with binding affinity −8.9 kcal/mol. The docking investigations were subsequently validated using co-crystallized ligand epitopes as positive controls. Molecular docking of MHC I alleles with co-crystallized ligand epitopes for HLA-A02:01, HLA-A24:02, and HLA-A07:02 yielded binding affinities of −9.3, −9.5, and −10 kcal/mol, respectively. Also, Molecular docking of MHC class II alleles with co-crystallized ligand epitopes for HLA-DRB1 and HLA-DP1 yielded binding affinities −9.7 and −9.3 kcal/mol, respectively. Molecular docking results showed that positive controls and selected epitopes have close binding similarities with HLA alleles.

According to pertinent investigations, the measure of binding energy is frequently employed to ascertain the probability of a ligand attaching itself to a protein target. The value of negative binding affinity indicates the strength and effectiveness of molecular interactions between ligand and receptor. This investigation reveals a strong correlation between T-cell epitopes and MHC allele-binding molecules, indicating a crucial role these interactions play in immune responses. Furthermore, the positive controls and all selected epitopes exhibited a substantial number of hydrophobic binding interactions with HLA alleles. A visual depiction of the interactions between the anticipated MHC molecules and epitopes is presented in Fig. 1.

3.3. Vaccine construct and evaluation of physicochemical properties

We meticulously combined and randomized epitope positions to design a vaccine construct comprising 200 amino acids. The complete vaccine sequence is displayed in Fig. 2A. Based on the predicted findings from ANTIGENpro and VaxiJen 2.0, the antigenicity amounts for the vaccine were 0.887 and 0.8691, respectively. The toxic and allergenic properties of the proposed vaccine were

Table 2
The selected HTL epitopes of CD204 and its immunogenic properties.

Epitope	Antigenicity	Allergenicity	Toxicity	IFN-γ	IL-4	MHCII alleles
NMEKRIQHILDMEAN	0.7049	Non allergen	Non-toxic	positive	IL4-inducer	DRB1_0404, HLA-DQA10102-DQB10501, HLA-DQA10102-DQB10604, HLA-DQA10103-DQB10501, HLA-DQA10103-DQB10603
HFQNFSMTTDQRFND	0.7423	Non allergen	Non-toxic	positive	IL4-inducer	DRB1_0701, HLA-DQA10102-DQB10604
EERVYNVSAEIMAMK	0.5619	Non allergen	Non-toxic	positive	IL4-inducer	DRB1_0901, HLA-DPA10103-DPB10301, HLA-DPA10103-DPB10601, HLA-DPA10103-DPB11101, HLA-DPA10103-DPB11701, HLA-DPA10103-DPB12001, HLA-DQA10201-DQB10201, HLA-DQA10201-DQB10202, HLA-DQA10501-DQB10201,
QQEEISKLEERVYNV	1.2442	Non allergen	Non-toxic	positive	IL4-inducer	DRB1_1201

Table 3
The selected LBL epitopes of CD204 and its immunogenic properties.

Epitope	Score	Antigenicity	Allergenicity	Toxicity
ANDITQSLTGKGNDSE	0.83	1.4040	Non allergen	Non-toxic
SSVQGHGNAIDEISKS	0.82	1.2278	Non allergen	Non-toxic

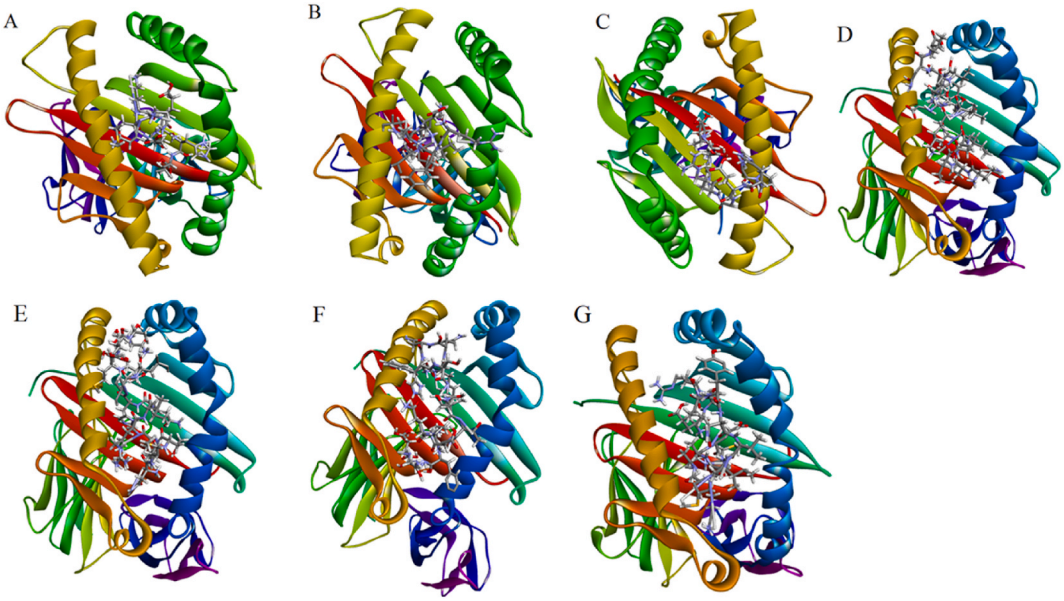

Fig. 1. The plot of the binding patterns between T-cell epitopes and their respective HLA binding alleles. (A) HLA-A*02:01-AMKEEQVHL complex; (B) HLA-A*24:02-RFNDILLQL complex; (C) HLA-A*07:02-GPHEGRVEI complex; (D) HLA-DRB1- QQEEISKLEERVYNV complex; (E) HLA-DRB1-NMEKRIQHILDMEAN complex; (F) HLA-DRB1- HFQNFSMTTDQRFND complex; (G) HLA-DP1- EERVYNVSAEIMAMK complex.

evaluated through ToxinPred and AllerTOP v2.0 tools and found to be non-toxic and non-allergenic. The evaluation of physico-chemical properties showed that the designed vaccine has a molecular weight of 21.95 kDa and a theoretical pI of 8.5. The vaccine instability index was calculated to be 37.58, which indicates an increase in protein stability. Furthermore, the aliphatic index, which indicates the proportion of aliphatic side chains in the structure, was measured at 63.95. A higher aliphatic index signifies enhanced thermostability, confirming the thermostable nature of the construct. This construct displayed a negative amount for the grand average of the hydrophobicity index (−0.743), which indicates a hydrophilic feature. This trait is desirable for a potential vaccine candidate. The half-life of the created vaccine in mammalian reticulocytes was 30 h, in yeast more than 20 h, and in *E. coli* more than 10 h. The likelihood that the vaccine will be soluble following overexpression in *E. coli* was determined to be 0.995706 based on predictions made by the SOLpro service. The absence of a signal peptide or transmembrane helix in the vaccine formulation suggests minimal

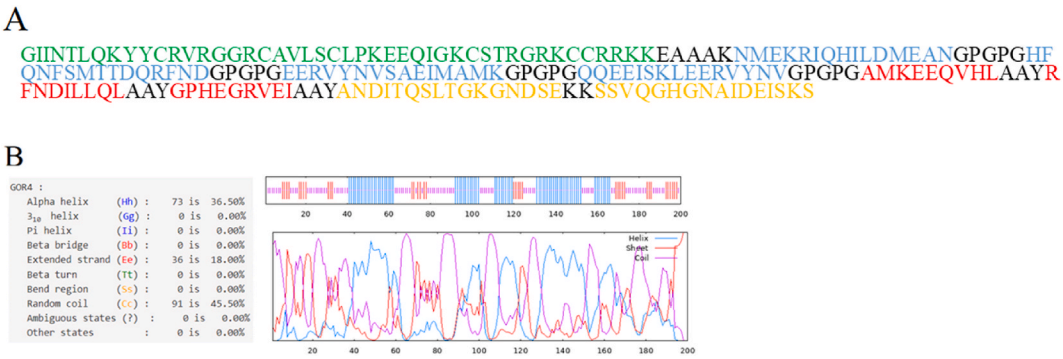

Fig. 2. The complete sequence of the vaccine construct. (A) The adjuvant is depicted green, the HTL epitopes are depicted blue, and the CTL epitopes are depicted red, The B-cell epitopes are depicted orange and all linkers are depicted black. (B) Prediction of the secondary structure of the final vaccine construct.

barriers to synthesis within living organisms, indicating a more efficient production process (Figs. S3 and S4).

3.4. Prediction of discontinuous B-cell epitope

Discontinuous B-cell epitopes within the designed vaccine's 3D structure were identified using the ElliPro tool. The tool identified five conformational B-cell epitopes within the vaccine protein, scoring between 0.807 and 0.599. These scores signify that antibodies will specifically recognize these regions, emphasizing their significance in humoral-mediated immunity (Table 4, Fig. 3).

3.5. Prediction and evaluation of secondary and tertiary structure of the vaccine construct

Predicting the secondary structure of a protein is crucial for understanding its function and creating a 3D model of its structure. The prabi server analysis revealed that the vaccine's secondary structure consisted of approximately 45.5 % coil, 36.5 % alpha-helix, and 18 % Extended strand (Fig. 2B). It's important to emphasize that proteins possessing coils and an alpha-helix are vital as structural antigens since antibodies can recognize them. Also, The formation of alpha helices and beta sheets can influence the accessibility and presentation of epitopes to the immune system. Proper folding ensures that epitopes are exposed on the surface, making them accessible to immune cells. Immune receptors, such as T-cell receptors or antibodies, are particularly adept at identifying specific secondary structures. They can recognize distinct patterns formed by alpha helices and beta sheets, thereby enhancing the immunological response. The vaccine's final three-dimensional configuration was predicted using the ROBETTA technology. Model 3 was the most suitable structure based on examining the SAVES tool. This selection was made based on the assessment of various parameters and criteria provided by the SAVES tool, which aided in determining the optimal model for the final vaccine structure. The model's general quality, assessed through ERRAT, scored 100. This service assesses protein structure accuracy and identifies correct and incorrect areas through atomic interactions; a high ERRAT number denotes desirable structural quality. The confirmation of the 3D representation demonstrates a high degree of compatibility for the examined model, as the Ramachandran plot analysis reveals that 98.2 % of the amino acid residues fall within the favored region. Moreover, over 90 % of the residues are situated in highly favorable areas, underscoring the high quality of the vaccine model. This model's general reliability and quality are shown by its Z-score of −7.81. Based on the above study's findings, the designed vaccine was shown to have a stable and reliable tertiary structure (Fig. 4). The tertiary structure of a vaccine ensures accurate presentation of epitopes, enabling the immune system to recognize and respond, and maintaining vaccine stability and effectiveness throughout storage and administration. The vaccine's three-dimensional arrangement affects its binding affinity to immune receptors like MHC molecules and T-cell receptors, crucial for a robust immune response. The tertiary structure ensures proper folding and exposure of antigenic sites, activating both innate and adaptive immune responses. The tertiary structure allows the vaccine to mimic the natural conformation of pathogen proteins. This mimicry helps the immune system recognize and respond to the vaccine as it would to an actual infection, enhancing the effectiveness of the immune response.

3.6. Molecular docking analysis of the vaccine with toll-like receptors

The construct was docked with immunological receptors such as TLR2 and TLR4. A series of 30 potential vaccine-TLR2 complex models were generated, each exhibiting distinct binding energies. The model with the lowest binding energy score (−895.1 kcal/mol) and the highest ranking was selected for further refining. Additionally, thirty vaccine-TLR4 model complexes were produced. The model with the highest ranking was elected based on its lowest binding energy score, which amounted to −881.0 kcal/mol. The HADDOCK program for the vaccine-TLR4 complex and vaccine-TLR2 complex were determined to be −156.1±10.0 and −208.0±17.1 kcal/mol, respectively. A low HADDOCK score indicates that vaccine and TLR binding is good. PDBsum analysis revealed that the TLR2 and vaccine formed 13 salt bridges and 36 hydrogen bonds, while TLR4 and the vaccine formed 7 salt bridges and 33 hydrogen bonds (Table S1).

As part of the vaccine-TLR2 complex, ARG43, LYS44, GLU92, LYS54, ARG55, ASP61, HIS71, GLU113, GLU114, GLU120 amino acid residues were involved in salt bridge formation, and VAL20, CYS23, GLY15, ARG17, ARG36, GLY88, ARG93, ARG36, ARG43, GLY90, GLU92, LYS54, ARG55, HIS58, HIS71, GLY70, ASN74, GLY66, PRO67, GLU113, GLN112, SER116, GLU114, ARG121 were implicated in the formation of hydrogen bonds (Fig. 5A). In the complex of the vaccine with TLR4, the formation of salt bridges involved specific amino acid residues from the vaccine, namely LYS199, ARG 160, GLU158, GLU92, ARG36, LYS 39, and ARG38, and

Table 4
Predicted conformational B-cell epitope residues from the designed vaccine.

No.	Residues	Number of residues	Score
1	B:R121, B:N124, B:V125, B:G126, B:P127, B:G128, B:P129, B:G130, B:A131, B:M132, B:K133, B:E134, B:E135, B:H138, B:T175, B:G176, B:K177, B:G178, B:N179, B:D180, B:S181, B:E182, B:K183, B:K184, B:S185, B:V187, B:Q188	27	0.807
2	B:R14, B:G15, B:G16, B:R17, B:C18, B:A19, B:V20, B:L21, B:C23, B:L24, B:P25, B:K26, B:E27, B:E28, B:Q29, B:I30, B:G31, B:K32, B:C33, B:S34, B:T35, B:R36, B:G37, B:R38, B:K39, B:C40, B:C41, B:R43	28	0.78
3	B:R160, B:V161, B:G191, B:N192, B:D195, B:E196, B:S198, B:K199	8	0.684
4	B:Q57, B:H58, B:L60, B:D61, B:M62, B:E63, B:A64, B:N65, B:G66, B:P67, B:G68, B:P69, B:G70, B:H71, B:F72, B:M104, B:K105	17	
5	B:D85, B:G86, B:P87, B:G88, B:P89, B:G90, B:E91, B:E92, B:R93	9	0.599

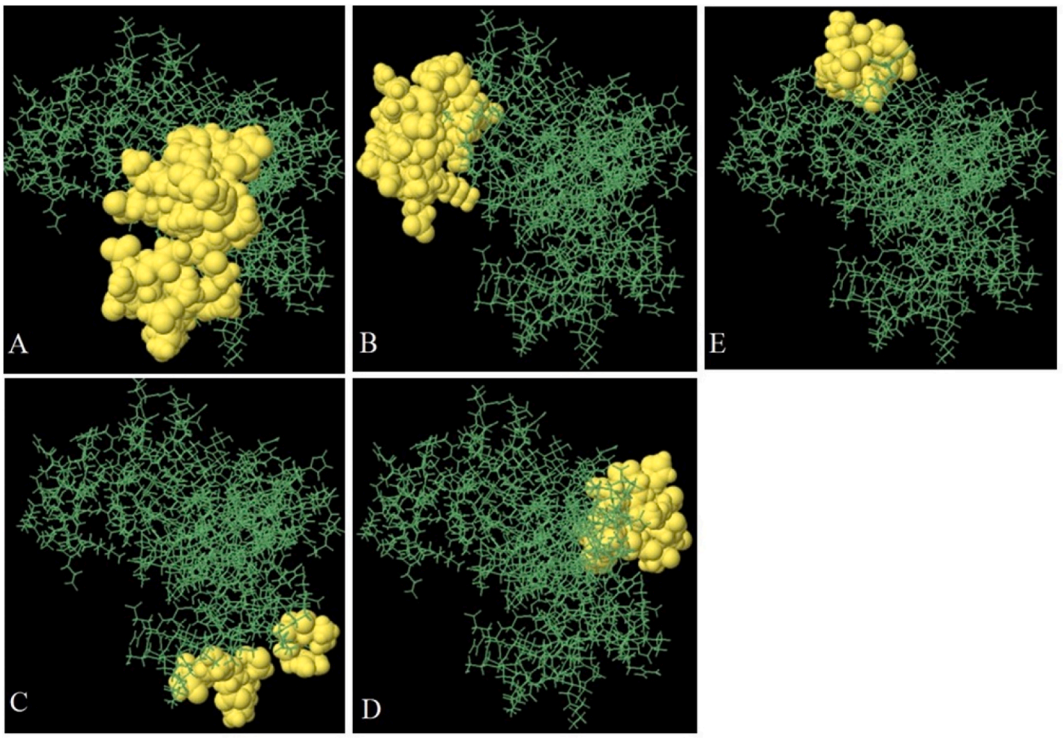

Fig. 3. 3D representation of discontinuous B-cell epitopes presents in the final vaccine. The epitopes are indicated by the yellow surface and the bulk of the protein is shown in gray sticks.

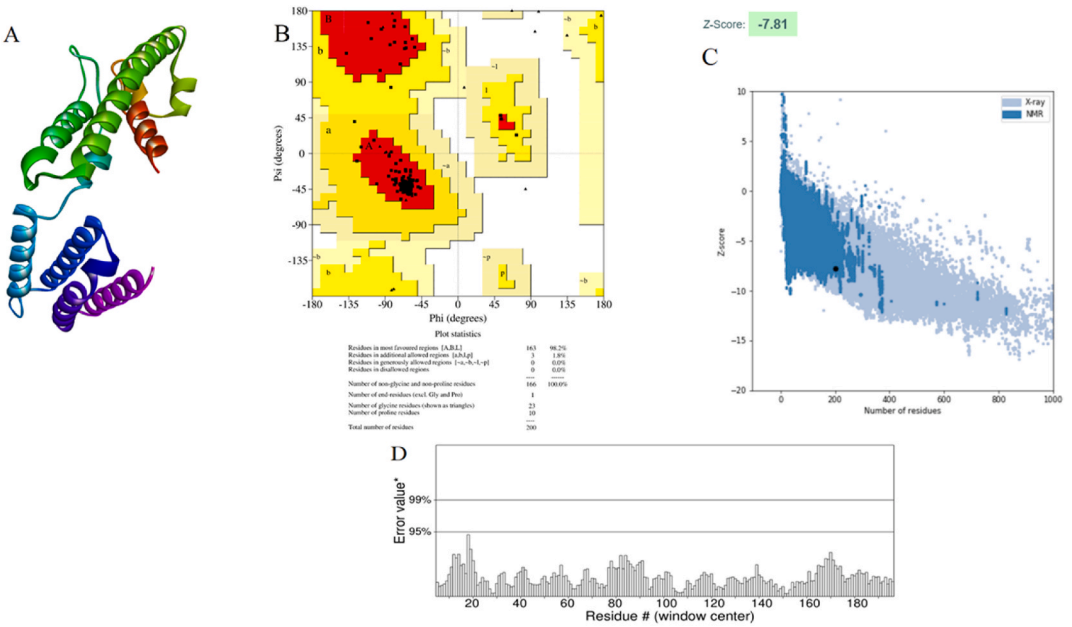

Fig. 4. (A) Robetta-generated 3D structure of the vaccine. (B) The Ramachandran plot of the 3D model generated by the PROCHECK server displays the most favored regions in red, additional allowed and generously allowed regions in dark yellow and light yellow, and disallowed regions in white. (C) The Z-score graph of the 3D model obtained via ProSA-web server. (D) The ERRAT diagram of the 3D model obtained via the ERRAT server.

the hydrogen bond formation implicated SER200, SER198, PRO156, HIS157, ARG160, GLY66, PRO66, GLY70, GLN73, ASN65, HIS71, ARG55, ASN74, ARG55, LYS54, LYS44, ARG43, LYS39, ARG36, ARG42, and THR35 within the vaccine (Fig. 5B). The above findings disclosed that the designed vaccine had great interactions with TLRs. (TLR4 and TLR2).

3.7. Molecular dynamics simulation

RMSD was used to evaluate the stability of the vaccine in the immunoreceptor binding site and as an indicator of conformational fluctuations between complexes. The RMSDs of vaccine-TLR2 and vaccine-TLR4 complexes showed noticeable and substantial fluctuations from the initiation of the simulation. The TLR2-vaccine complex achieved stability after 10 ns and stayed stable until the completion of the simulation, whereas the TLR4-vaccine complex achieved stability after 20 ns and continued stable until the end. The RMSD amounts for TLR2-vaccine and TLR4-vaccine complexes were in the range of 0.2–0.4 nm (average 0.3384 nm) and approximately in the range of 0.2–0.8 nm (average 0.7006 nm), respectively, which represents the stability of the structures of the complexes (Fig. 6 A). The RMSF characterizes the fluctuation of protein residues about a fixed reference point throughout a simulation period. In both complexes, no typical fluctuations in the TLR structure were observed. While in vaccine structures in both systems the loop regions (120-13, 16–21, and 176–179) a small fluctuation was observed. The examination of the entirety of the solvent-accessible surface region demonstrated the alteration in the surface area of the complex concerning the progression of time. The mean values of SASA for the TLR2-vaccine were found to be 351.46 nm\S2\N and the TLR4-vaccine to be 373.54 nm\S2\N. The trend of the SASA plot showed an inverse relationship to that of RMSD, thereby suggesting that a more favorable interaction between the receptor and ligand resulted in a decrease in the surface region of the protein complexes (Fig. 6B). The findings of the SASA evaluation once again demonstrated a consistent interaction between TLRs (TLR2 and TLR4) and the vaccine protein. The number of hydrogen bonds established over the trajectory between a ligand and protein is displayed on the H-bond plot. On average, 15 and 12 H-bonds were composed between the TLR2-vaccine and TLR4-vaccine, respectively (Fig. 6C). A great affinity for TLRs was indicated by the presence of hydrogen bonds in the vaccine. Additionally, the binding stability of the docked molecule was evaluated utilizing rGyr. Higher folded stability is indicated by a more condensed complex, which is shown by a lower rGyr value (Fig. 6D). It's worth mentioning that the average Rg of the vaccine construct when bound to the TLR-2 receptor was smaller than that of the TLR-4 vaccine construct complex. This disparity indicates an increase in structural compactness following the binding process. In the biological system, a low Rg profile indicates greater rigidity. The calculation of the binding free energies between the receptor complexes (TLR2 and TLR4) and the vaccine was conducted utilizing the MMPBSA method. The vaccine-TLR2 and vaccine-TLR4 complexes exhibited binding energy values of −113.41 and −106.61 kcal/mol, respectively. Overall, the data indicate that the vaccine has a greater binding preference for TLR2 over TLR4. The stability of vaccine-TLR complexes plays a vital role in determining their immunogenicity and effectiveness in practical applications. The behavior of these complexes, encompassing variations and stability parameters, can profoundly affect the functional results of vaccines. A comprehensive understanding of these interactions can enhance vaccine design and significantly improve overall efficacy. Stable vaccine-TLR complexes ensure sustained immune activation, which is essential for robust responses. Fluctuations in complex stability represented by RMSF values can lead to irregular immune activation. Such abnormalities may affect

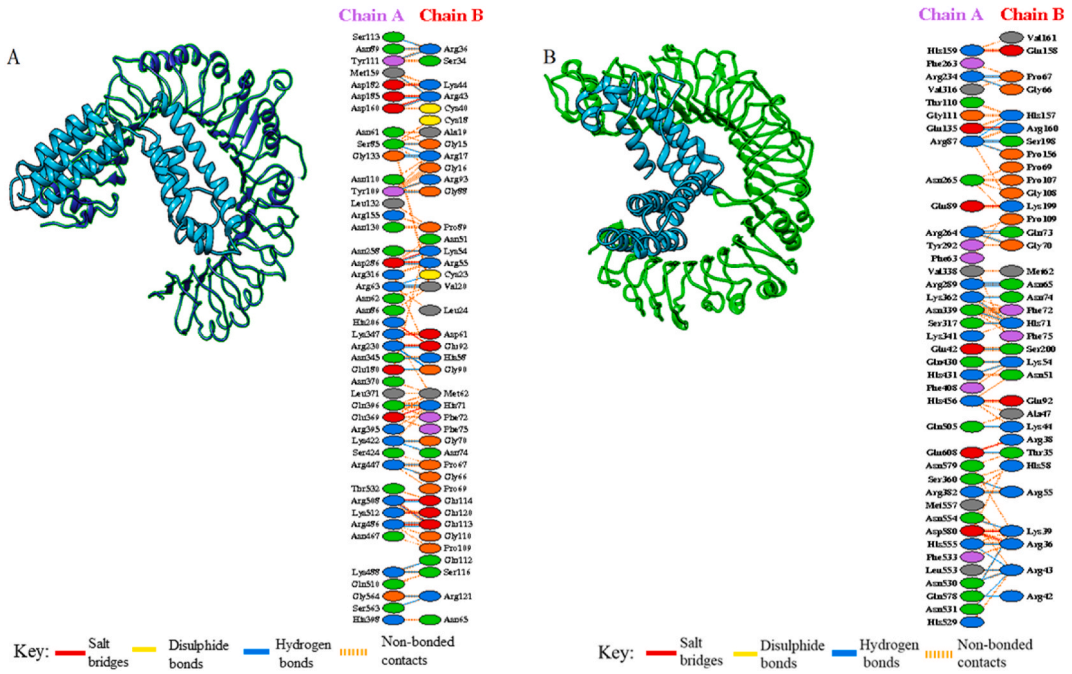

Fig. 5. The plot of visualized analysis and the interacting amino acid residues of the docking complex. The TLR2 receptor exhibits a medium blue coloration, while the TLR4 receptor displays a green hue, and the vaccine is characterized by a cyan shade. (A) The visualization of the TLR2 and vaccine complex along with residues that interact with them. In this context, Chain A denotes the TLR2 receptor, while Chain B represents the vaccine. (B) The visualization of the TLR4 and vaccine complex along with residues that interact with them. In this context, Chain A denotes the TLR2 receptor, while Chain B represents the vaccine.

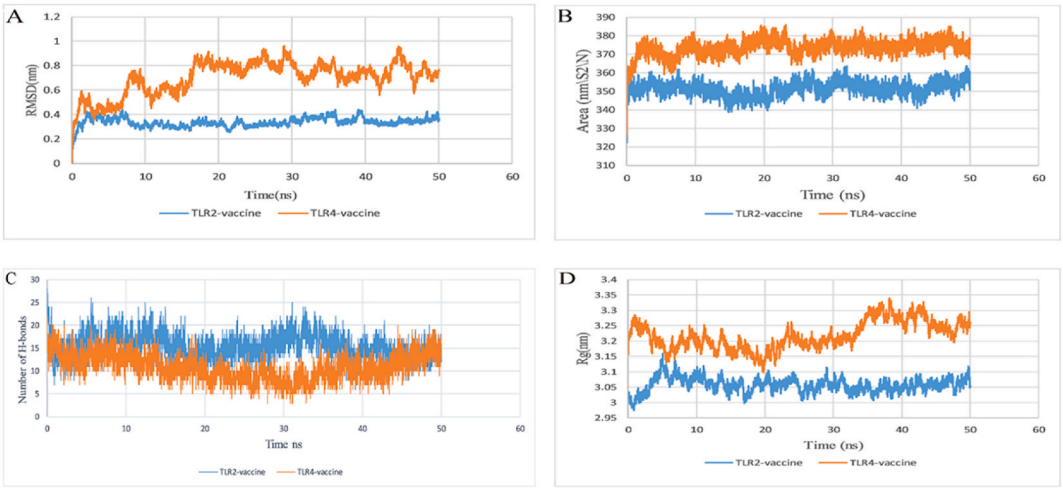

Fig. 6. The analysis of molecular dynamics simulation of vaccine and TLR2/4 complex at 50ns. (A) The RMSD plot of the docked TLR and vaccine complexes; (B) The SASA profile of the different TLRs and vaccine during the simulation; (C) Hydrogen bonds formed between the TLR2/4 and vaccine (D) Radius of Gyration plots of the docked TLR and vaccine complexes.

the synthesis of essential cytokines that play an important role in coordinating immune responses. The stability metrics observed are associated with the vaccine's capacity to induce robust Th1-polarized immune responses, as demonstrated in research employing nanoscale patterning of TLR ligands [66].

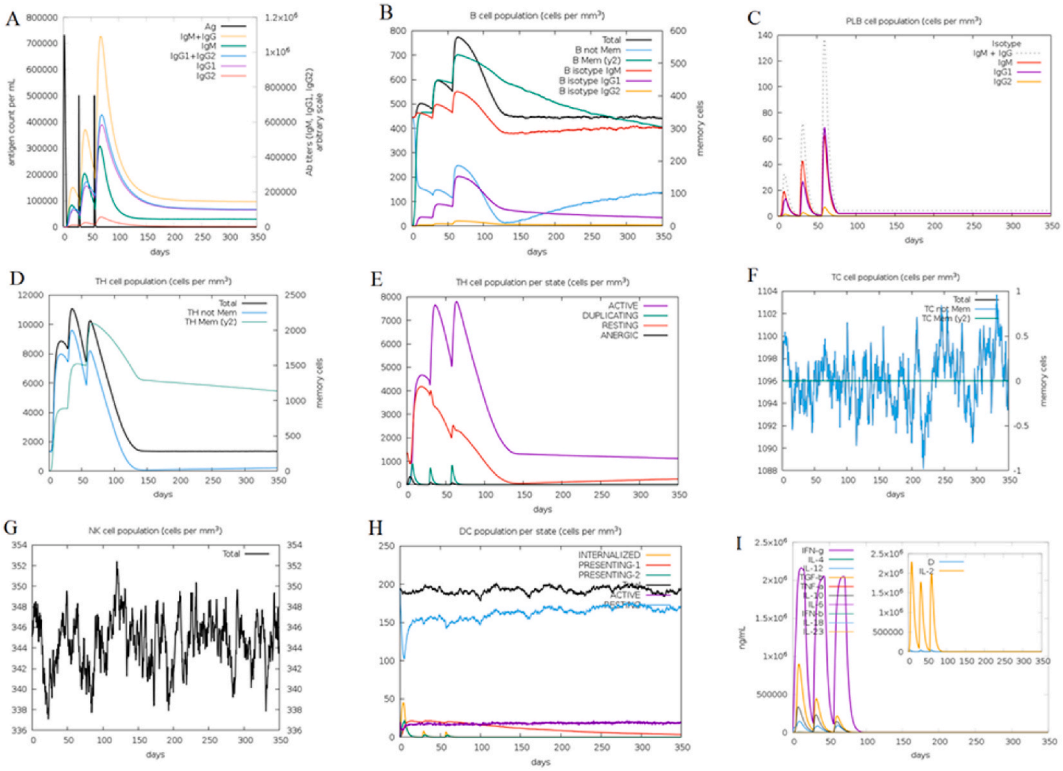

Fig. 7. Immune response spectrum of the vaccine construct. (A) The evolution of immunoglobulin concentration after three injections; (B) The evolution of B cell population after three injections; (C) The evolution of plasma B-cell population after three injections; (D) The evolution of helper T cell population after three injections; (E) The evolution of helper T cell population per state after three injections; (F) The evolution of cytotoxic T cell population per state after three injections; (G) The evolution of natural killer (NK) cell population after three injections; (H) The evolution of dendritic cells (DC) population per state after three injections; (I) The evolution of IFN-γ concentration and IL-4, IL6 and IL12 after three injections.

3.8. Immune simulation

The vaccine's immune-boosting effect was achieved through the utilization of the CImmSim online platform, which forecasts the potential of the vaccine to prompt substantial adaptive immune responses within the human organism. After the initial injection, a decline in lgM antibody titers, a decrease in the lgM B-cell isotypes, and a minor presence of the lgG B-cell isotypes were noted. After the second and third injections, elevated IgM antibody levels accompanied by IgG1+IgG2, IgG1, and IgG + IgM were observed, as well as a noticeable presence of memory B cells (Fig. 7A and B). Furthermore, the active, memory, and total numbers of TH-cells enhanced during the secondary and tertiary phases of the immune response, alongside B-cells and plasma B-cells (Fig. 7B–E). Throughout the immune stimulation, cytotoxic T lymphocytes (TC cells) were noted, reaching a peak of 1105 cells per mm3 (Fig. 7F). Furthermore, the vaccine exposure led to the activation of both NK and Dendritic Cells (Fig. 7G and H). The vaccine elicited the activation of a diverse array of cytokines, including IL-4, IL-2, and INF-γ, as illustrated in Fig. 7I. Furthermore, the formulated vaccine effectively stimulated a significant increase in both immune cell production and a wide range of cytokines. These findings indicate its potential to successfully elicit both adaptive and memory immune responses within the host.

3.9. Codon optimization and in silico cloning vaccine construct

To enhance the codon usage of the vaccine design for maximum protein production in *E. coli* strain K12, we utilized the Java Codon Adaptation program (JCat). The length of this codon sequence was 600 nucleotides. A codon adaptive index (CAI) of 1.0 was calculated for the refined nucleotide sequence, and an average GC content of 50.3 % was found in the adapted sequence. These data suggest that the vaccine candidate has the possibility for successful expression within the *E. coli* host. For GC content, the ideal value is between 30 and 70 %. Using the SnapGene program, the modified codon sequence was engineered and incorporated into the recombinant plasmid's pET30a(+) vector sequence (Fig. 8).

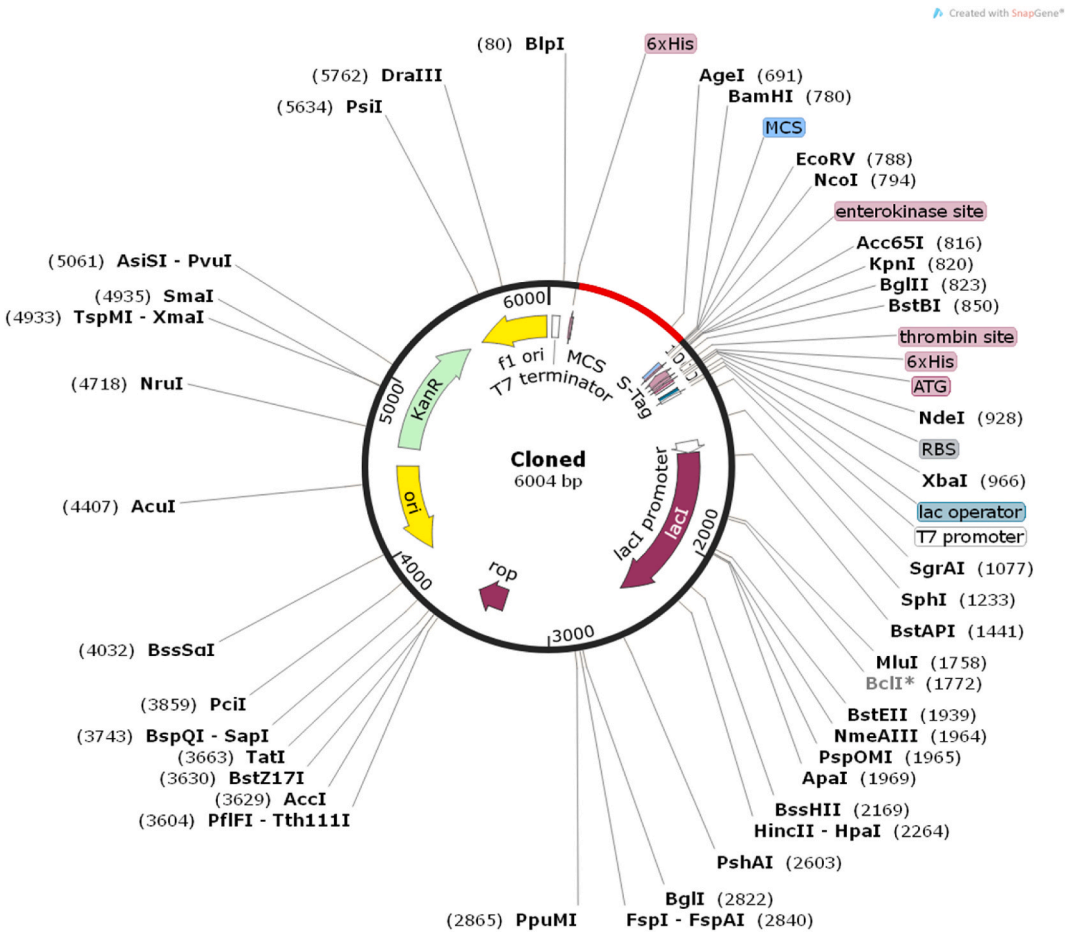

Fig. 8. Cloning of the optimized DNA sequence of the proposed vaccine in the pET30a(+) expression system.

4. Discussion

In this research, we propose a novel strategy to develop a vaccine for glioblastoma. Since CD204 plays a critical role in the tumor microenvironment, it is an attractive target for glioblastoma and a marker for M2-polarized tumor-associated macrophages [13]. Research has demonstrated that CD204 expression increases with malignancy grade and is linked to a worse survival rate in high-grade gliomas. Furthermore, CD204 stands out as a strong candidate for therapeutic intervention due to its identification as an independent predictive factor in glioblastoma [67]. Recent studies have demonstrated that CD204 has immunomodulatory properties that inhibit both systemic and local immunity, which accelerates the growth of tumors. By targeting CD204, it may be possible to interfere with these immunosuppressive processes and enhance the immune system's ability to combat glioblastoma cells [13]. In conclusion, the strong association of CD204 with tumor growth and poor prognosis in glioblastoma patients, along with its potential to enhance the efficacy of immunotherapy, justifies its selection as a therapeutic target [67]. The designed vaccine is based on multiple epitopes, which are specific parts of the tumor-associated macrophage CD204 protein. We aim to stimulate an immune response against glioblastoma cells by targeting this protein. This study offers a comprehensive perception of the initial phase of vaccine development, including the identification of potential immunogenic targets. Epitope selection is a significant stage in the development of multi-epitope vaccines. In this research, an assessment was conducted on the toxicity, allergenicity, and antigenicity of all projected epitopes. Accordingly, we have identified four HTL epitopes, three CTL epitopes, and two B lymphocyte epitopes, all of which hold great potential as promising targets for the development of a vaccine. Various linkers were employed to join epitopes with diverse arrangements in multiple primary structures of the vaccine construct. After examining the physicochemical attributes, specifically regarding the durability of the formed structures, it was determined that the GPGPG, AAY, and KK linkers are suitable for connecting HTL, CTL, and linear B-cell epitopes, respectively. Adjuvants can not only enhance the multi-epitope vaccine's immunogenicity but also can induce a long-lasting immune response [68]. In this investigation, the inclusion of b-defensin in the structure of the vaccine as an adjuvant aimed to diminish the toxicity and boost the overall antibody response systemically when delivered alongside antigens [18]. The physicochemical properties of the vaccine were assessed to accelerate additional experimental assessments of the vaccine and to ensure the effective execution of in vivo and in vitro trials. The vaccine's hypothetical isoelectric point (pI) was ascertained to be 8.50, implying that the vaccine possesses an alkaline feature. The engineered vaccine has a negative GRAVY score (−0.743). This measurement demonstrates the hydrophilic trait of the vaccine and its remarkable solubility. The molecular weight of the vaccine was established at 21.95 kDa. Vaccines with molecular weights below 110 kDa were considered favorable candidates, as they are more straightforward to clone and express in expression systems compared to larger proteins [69]. The aliphatic index value of 63.95 exhibits that the vaccine possesses stability at higher temperatures, as an aliphatic index exceeding 50 serves as a threshold for such stability [70]. The vaccine appears to be stable based on its observed instability index of 37.58. When the protein's instability index is less than 40, it is generally considered stable [46].

Moreover, the vaccine exhibited greater solubility compared to the soluble *E. coli* proteins in the experimental dataset [47,71]. Evaluation of antigenicity and allergenicity after vaccine design showed a significant level of antigenicity (0.8) while it lacked allergenic properties and showed intrinsic non-toxicity. As shown in the Ramachandran plot, most amino acid residues are present in the favored or additionally allowed regions, whereas residues were not found within the region that is disallowed. This finding implies that the predicted model possesses a remarkable level of quality. Moreover, the ProSA tool was employed to examine the model structure for potential errors. The resulting Z-score of −7.81 indicates that the overall construct of the model is reliable and of high quality. The initiation of the immune response requires a robust interaction between the immune receptor molecule and, the antigenic molecule specifically TLR2 and TLR4 [64,72]. Based on the binding analysis results, we have identified stable associations and strong affinity between TLRs and the multi-epitope vaccine. This indicates that the designed vaccine can successfully stimulate the immune response.

A consistent degree of stability was observed during the 50ns simulation of the TLR2-vaccine complex based on RMSD results. Regarding the RMSD trend of the TLR4-vaccine complex, all RMSDs achieved equilibrium at 20ns in the simulations, even with the changes that were reached during the simulation. The Rg amounts of two systems comprising TLR-vaccine complexes also displayed a tendency to reach a stable state after a duration of 10 ns. This observation provides additional evidence to support the notion of the complex being stable. Moreover, throughout all MD simulations, a greater number of hydrogen bonds were established within the TLR4 vaccine and TLR2 vaccine complexes, resulting in the vaccine chain binding to TLR4 and TLR2 chains with significant affinity. The MM-PBSA examination revealed that a minimal amount of energy was necessary to maintain the stability of the two complexes.

The research mentioned above shows that the newly developed vaccine can firmly bind to TLRs and effectively engage the host's immune system, leading to a strong immunological reaction. Throughout the simulation of the immune response, an increase in the number of TC cells, TH cells, and B cells was noticed, along with the generation of IgA, IgG, IL-2, IFN-γ, and several other cytokines following the administration of the vaccine. Moreover, recurrent administration of the vaccine leads to the recognition of memory B cells, indicating that the vaccine could stimulate both humoral and cellular immunity. To validate the expression of the vaccine, codon optimization, and cloning techniques were used to assess the feasibility of large-scale production. The calculated amounts of GC content and CAI suggested the potential for effective expression of the proposed vaccine in the *E. coli* K12 strain. Peptide-based cancer vaccines, developed via in silico methods, represent a breakthrough in cancer immunotherapy, leveraging computational techniques to design and evaluate the efficacy of immunogenic peptides. These vaccines employ antigens derived from tumors to provoke immune responses, and recent developments have improved their predictive accuracy and effectiveness in trials conducted on both mice and humans. In vivo studies have demonstrated that multiepitope vaccines can significantly enhance immune responses and inhibit tumor growth in mouse models. For example, co-immunization with DNA and peptide vaccines led to substantial tumor growth inhibition and increased survival rates in mice with mammary carcinoma [73]. The favorable outcomes observed in preclinical research imply that

these in-silico-developed vaccines could be implemented in clinical practice, potentially presenting new treatment possibilities for cancer patients. Ongoing clinical trials are exploring their safety and efficacy in humans [26]. Vaccination with glioma-associated antigens (TAAs) such as EphA2 and IL-13Rα2 has been shown to activate T-cell responses in pediatric patients, particularly those with brainstem gliomas [74]. Studies indicate that personal neoantigen vaccines, such as NeoVax, can elicit long-lasting T cell responses, with patients demonstrating neoantigen-specific T cells exhibiting a memory phenotype even after several years post-vaccination [75]. The clinical study of the survivin long peptide vaccine, SurVaxM, in patients with recurrent malignant glioma has shown promising results regarding safety, immunogenicity, and clinical efficacy [76].

In silico peptide-based vaccines have various disadvantages, including limited immunogenicity of simple peptides, which may demand the introduction of adjuvants to excite T cells and build immunological memory. In addition, these vaccines are prone to issues including inadequate solubility, a short circulating half-life, and a tendency to undergo proteolytic degradation. These factors can significantly influence their efficacy and effectiveness in eliciting a robust immune response. The next step is to produce this protein vaccine in a bacterial system and perform the various immunological assays needed to validate the findings from the immunoinformatics analysis. However, the findings of this investigation present a robust basis for additional in vitro and in vivo research endeavors aimed at illustrating the effectiveness and safety of the structure.

5. Conclusion

This study developed an epitope-based peptide vaccine against GBM by fusing epitopes that can stimulate immunity via both humoral and cell-mediated mechanisms with an adjuvant, β-defensin 3. The results obtained from computational tools confirmed that the designed vaccine exhibits high stability and a strong capability to induce a sustained immune response. Although our study's results indicate that the developed multi-epitope vaccine may serve as a promising therapeutic option for GBM. These findings must be validated through rigorous experimental and animal studies before advancing to human trials.

CRediT authorship contribution statement

Reza Salahlou: Writing – original draft, Visualization, Validation, Supervision, Software, Resources, Methodology, Investigation, Formal analysis, Data curation, Conceptualization. **Safar Farajnia:** Writing – review & editing, Visualization, Validation, Supervision, Software, Resources, Project administration, Methodology, Investigation, Funding acquisition, Formal analysis, Data curation. **Effat Alizadeh:** Writing – review & editing, Validation, Supervision, Investigation. **Siavoush Dastmalchi:** Writing – review & editing, Visualization, Validation, Supervision, Resources, Methodology. **Nasrin Bargahi:** Writing – review & editing, Visualization, Validation. **Leila Rahbarnia:** Writing – review & editing, Visualization, Validation, Investigation. **Safooreh Hoseinpour Steyar:** Writing – original draft, Visualization, Validation, Methodology, Investigation.

Data availability statement

The dataset supporting the conclusions of this article is included within the article (and its additional files).

Ethics approval and consent to participate

This work was approved by the Ethical Committee of Tabriz University of Medical Sciences, Tabriz, Iran (IR.TBZMED.AEC.1400.016).

Consent for publication

Not applicable.

Declaration of competing interest

The authors declare the following financial interests/personal relationships which may be considered as potential competing interests: Safar Farajnia reports financial support was provided by Tabriz University of Medical Sciences Biotechnology Research Centre. If there are other authors, they declare that they have no known competing financial interests or personal relationships that could have appeared to influence the work reported in this paper.

Abbreviations

GBM	Glioblastoma multiforme
CTL	Cytotoxic T lymphocyte
HTL	Helper T lymphocyte
MSR1	Macrophage Scavenger Receptor 1
TAMs	Tumor-associated macrophages
IFN-γ	Interferon gamma

IL-4	Interleukin-4
CAI	Codon adaptation index
HLA	Human leukocyte antigen
ANNs	Artificial neural networks
TH1	T Helper 1 cells
RMSD	Root mean square deviation
TLR-2	Toll-like receptor 2
TLR-4	Toll-like receptor 4
PDB	Protein data bank
IEDB	Immune Epitope Database
RMSF	Root means square function
SASA	Solvent accessible surface area

Appendix A. Supplementary data

Supplementary data to this article can be found online at https://doi.org/10.1016/j.heliyon.2024.e40774.

References

[1] S. Tamai, T. Ichinose, T. Tsutsui, S. Tanaka, F. Garaeva, H. Sabit, et al., Tumor microenvironment in glioma invasion, Brain Sci. 12 (2022), https://doi.org/10.3390/brainsci12040505.

[2] E. Agosti, P.P. Panciani, M. Zeppieri, L. De Maria, F. Pasqualetti, A. Tel, et al., Tumor microenvironment and glioblastoma cell interplay as promoters of therapeutic resistance, Biology 12 (2023), https://doi.org/10.3390/biology12050736.

[3] M.B. Graeber, B.W. Scheithauer, G.W. Kreutzberg, Microglia in brain tumors, Glia 40 (2002) 252–259, https://doi.org/10.1002/glia.10147.

[4] R.L. Bowman, F. Klemm, L. Akkari, S.M. Pyonteck, L. Sevenich, D.F. Quail, et al., Macrophage ontogeny underlies differences in tumor-specific education in brain malignancies, Cell Rep. 17 (2016) 2445–2459, https://doi.org/10.1016/j.celrep.2016.10.052.

[5] A.C. da Fonseca, B. Badie, Microglia and macrophages in malignant gliomas: recent discoveries and implications for promising therapies, Clin. Dev. Immunol. 2013 (2013) 264124, https://doi.org/10.1155/2013/264124.

[6] Y. Yuan, Q. Zhao, S. Zhao, P. Zhang, H. Zhao, Z. Li, et al., Characterization of transcriptome profile and clinical features of a novel immunotherapy target CD204 in diffuse glioma, Cancer Med. 8 (2019) 3811–3821, https://doi.org/10.1002/cam4.2312.

[7] X.Z. Ye, S.L. Xu, Y.H. Xin, S.C. Yu, Y.F. Ping, L. Chen, et al., Tumor-associated microglia/macrophages enhance the invasion of glioma stem-like cells via TGF-β1 signaling pathway, J. Immunol. 189 (2012) 444–453, https://doi.org/10.4049/jimmunol.1103248.

[8] R.K. Jain, E. di Tomaso, D.G. Duda, J.S. Loeffler, A.G. Sorensen, T.T. Batchelor, Angiogenesis in brain tumours, Nat. Rev. Neurosci. 8 (2007) 610–622, https://doi.org/10.1038/nrn2175.

[9] S.K. Biswas, M. Chittezhath, I.N. Shalova, J.Y. Lim, Macrophage polarization and plasticity in health and disease, Immunol. Res. 53 (2012) 11–24, https://doi.org/10.1007/s12026-012-8291-9.

[10] A.L. Chang, J. Miska, D.A. Wainwright, M. Dey, C.V. Rivetta, D. Yu, et al., CCL2 produced by the glioma microenvironment is essential for the recruitment of regulatory T cells and myeloid-derived suppressor cells, Cancer Res. 76 (2016) 5671–5682, https://doi.org/10.1158/0008-5472.Can-16-0144.

[11] L. Rohrer, M. Freeman, T. Kodama, M. Penman, M. Krieger, Coiled-coil fibrous domains mediate ligand binding by macrophage scavenger receptor type II, Nature 343 (1990) 570–572, https://doi.org/10.1038/343570a0.

[12] J.L. Kelley, T.R. Ozment, C. Li, J.B. Schweitzer, D.L. Williams, Scavenger receptor-A (CD204): a two-edged sword in health and disease, Crit. Rev. Immunol. 34 (2014) 241–261, https://doi.org/10.1615/critrevimmunol.2014010267.

[13] M. Kurdi, B. Alghamdi, N.S. Butt, S. Baeesa, The relationship between CD204 (M2)-polarized tumour-associated macrophages (TAMs), tumour-infiltrating lymphocytes (TILs), and microglial activation in glioblastoma microenvironment: a novel immune checkpoint receptor target, Discov Oncol 12 (2021) 28, https://doi.org/10.1007/s12672-021-00423-8.

[14] J. Xiong, X. Zhou, L. Su, L. Jiang, Z. Ming, C. Pang, et al., The two-sided battlefield of tumour-associated macrophages in glioblastoma: unravelling their therapeutic potential, Discov Oncol 15 (2024) 590, https://doi.org/10.1007/s12672-024-01464-5.

[15] M. Prosniak, L.A. Harshyne, D.W. Andrews, L.C. Kenyon, K. Bedelbaeva, T.V. Apanasovich, et al., Glioma grade is associated with the accumulation and activity of cells bearing M2 monocyte markers, Clin. Cancer Res. 19 (2013) 3776–3786, https://doi.org/10.1158/1078-0432.Ccr-12-1940.

[16] T. Fan, M. Zhang, J. Yang, Z. Zhu, W. Cao, C. Dong, Therapeutic cancer vaccines: advancements, challenges, and prospects, Signal Transduct Target Ther 8 (2023) 450, https://doi.org/10.1038/s41392-023-01674-3.

[17] P. Paranthaman, S. Veerappapillai, Design of a potential Sema4A-based multi-epitope vaccine to combat triple-negative breast cancer: an immunoinformatic approach, Med. Oncol. 40 (2023) 105, https://doi.org/10.1007/s12032-023-01970-6.

[18] V. Dhople, A. Krukemeyer, A. Ramamoorthy, The human beta-defensin-3, an antibacterial peptide with multiple biological functions, Biochim. Biophys. Acta 1758 (2006) 1499–1512, https://doi.org/10.1016/j.bbamem.2006.07.007.

[19] Y. Wu, L. Feng, Biomaterials-assisted construction of neoantigen vaccines for personalized cancer immunotherapy, Expert Opin Drug Deliv 20 (2023) 323–333, https://doi.org/10.1080/17425247.2023.2168640.

[20] S. Zanotta, D. Galati, R. De Filippi, A. Pinto, Enhancing dendritic cell cancer vaccination: the synergy of immune checkpoint inhibitors in combined therapies, Int. J. Mol. Sci. 25 (2024), https://doi.org/10.3390/ijms25147509.

[21] K. Savsani, S. Dakshanamurthy, Novel methodology for the design of personalized cancer vaccine targeting neoantigens: application to pancreatic ductal adenocarcinoma, Diseases 12 (2024), https://doi.org/10.3390/diseases12070149.

[22] Z.S. Chheda, G. Kohanbash, K. Okada, N. Jahan, J. Sidney, M. Pecoraro, et al., Novel and shared neoantigen derived from histone 3 variant H3.3K27M mutation for glioma T cell therapy, J. Exp. Med. 215 (2018) 141–157, https://doi.org/10.1084/jem.20171046.

[23] A. Saijo, H. Ogino, N.A. Butowski, M.R. Tedesco, D. Gibson, P.B. Watchmaker, et al., A combinatory vaccine with IMA950 plus varlilumab promotes effector memory T-cell differentiation in the peripheral blood of patients with low-grade gliomas, Neuro Oncol. 26 (2024) 335–347, https://doi.org/10.1093/neuonc/noad185.

[24] I.N. Lu, S. Farinelle, A. Sausy, C.P. Muller, Identification of a CD4 T-cell epitope in the hemagglutinin stalk domain of pandemic H1N1 influenza virus and its antigen-driven TCR usage signature in BALB/c mice, Cell. Mol. Immunol. 14 (2017) 511–520, https://doi.org/10.1038/cmi.2016.20.

[25] R. He, X. Yang, C. Liu, X. Chen, L. Wang, M. Xiao, et al., Efficient control of chronic LCMV infection by a CD4 T cell epitope-based heterologous prime-boost vaccination in a murine model, Cell. Mol. Immunol. 15 (2018) 815–826, https://doi.org/10.1038/cmi.2017.3.

[26] S. Sotirov, I. Dimitrov, Tumor-derived antigenic peptides as potential cancer vaccines, Int. J. Mol. Sci. 25 (2024), https://doi.org/10.3390/ijms25094934.

[27] B. Reynisson, B. Alvarez, S. Paul, B. Peters, M. Nielsen, NetMHCpan-4.1 and NetMHCIIpan-4.0: improved predictions of MHC antigen presentation by concurrent motif deconvolution and integration of MS MHC eluted ligand data, Nucleic Acids Res. 48 (2020), https://doi.org/10.1093/nar/gkaa379. W449-w54.

[28] B. Reynisson, C. Barra, S. Kaabinejadian, W.H. Hildebrand, B. Peters, M. Nielsen, Improved prediction of MHC II antigen presentation through integration and motif deconvolution of mass spectrometry MHC eluted ligand data, J. Proteome Res. 19 (2020) 2304–2315, https://doi.org/10.1021/acs.jproteome.9b00874.

[29] S. Saha, G.P. Raghava, Prediction methods for B-cell epitopes, Methods Mol. Biol. 409 (2007) 387–394, https://doi.org/10.1007/978-1-60327-118-9_29.

[30] J. Ponomarenko, H.H. Bui, W. Li, N. Fusseder, P.E. Bourne, A. Sette, et al., ElliPro: a new structure-based tool for the prediction of antibody epitopes, BMC Bioinf. 9 (2008) 514, https://doi.org/10.1186/1471-2105-9-514.

[31] I. Dimitrov, L. Naneva, I. Doytchinova, I. Bangov, AllergenFP: allergenicity prediction by descriptor fingerprints, Bioinformatics 30 (2014) 846–851, https://doi.org/10.1093/bioinformatics/btt619.

[32] S. Gupta, P. Kapoor, K. Chaudhary, A. Gautam, R. Kumar, G.P. Raghava, In silico approach for predicting toxicity of peptides and proteins, PLoS One 8 (2013) e73957, https://doi.org/10.1371/journal.pone.0073957.

[33] J.J. Calis, M. Maybeno, J.A. Greenbaum, D. Weiskopf, A.D. De Silva, A. Sette, et al., Properties of MHC class I presented peptides that enhance immunogenicity, PLoS Comput. Biol. 9 (2013) e1003266, https://doi.org/10.1371/journal.pcbi.1003266.

[34] S. Paul, J. Sidney, A. Sette, B. Peters, TepiTool: a pipeline for computational prediction of T cell epitope candidates, Curr. Protoc. Im. 114 (2016), https://doi.org/10.1002/cpim.12, 18.9.1-.9.24.

[35] G. Kak, M. Raza, B.K. Tiwari, Interferon-gamma (IFN-γ): exploring its implications in infectious diseases, Biomol. Concepts 9 (2018) 64–79, https://doi.org/10.1515/bmc-2018-0007.

[36] C.A. Dinarello, Historical insights into cytokines, Eur. J. Immunol. 37 (Suppl 1) (2007) S34–S45, https://doi.org/10.1002/eji.200737772.

[37] S.K. Dhanda, P. Vir, G.P. Raghava, Designing of interferon-gamma inducing MHC class-II binders, Biol. Direct 8 (2013) 30, https://doi.org/10.1186/1745-6150-8-30.

[38] S.K. Dhanda, S. Gupta, P. Vir, G.P. Raghava, Prediction of IL4 inducing peptides, Clin. Dev. Immunol. 2013 (2013) 263952, https://doi.org/10.1155/2013/263952.

[39] A. Lamiable, P. Thévenet, J. Rey, M. Vavrusa, P. Derreumaux, P. Tufféry, PEP-FOLD3: faster de novo structure prediction for linear peptides in solution and in complex, Nucleic Acids Res. 44 (2016) W449–W454, https://doi.org/10.1093/nar/gkw329.

[40] J.L. Sussman, D. Lin, J. Jiang, N.O. Manning, J. Prilusky, O. Ritter, et al., Protein Data Bank (PDB): database of three-dimensional structural information of biological macromolecules, Acta Crystallogr D Biol Crystallogr 54 (1998) 1078–1084, https://doi.org/10.1107/s0907444998009378.

[41] N. Guex, M.C. Peitsch, T. Schwede, Automated comparative protein structure modeling with SWISS-MODEL and Swiss-PdbViewer: a historical perspective, Electrophoresis 30 (Suppl 1) (2009) S162–S173, https://doi.org/10.1002/elps.200900140.

[42] O. Trott, A.J. Olson, AutoDock Vina: improving the speed and accuracy of docking with a new scoring function, efficient optimization, and multithreading, J. Comput. Chem. 31 (2010) 455–461, https://doi.org/10.1002/jcc.21334.

[43] Z. Nain, F. Abdulla, M.M. Rahman, M.M. Karim, M.S.A. Khan, S.B. Sayed, et al., Proteome-wide screening for designing a multi-epitope vaccine against emerging pathogen Elizabethkingia anophelis using immunoinformatic approaches, J. Biomol. Struct. Dyn. 38 (2020) 4850–4867, https://doi.org/10.1080/07391102.2019.1692072.

[44] H. Dorosti, M. Eslami, M. Negahdaripour, M.B. Ghoshoon, A. Gholami, R. Heidari, et al., Vaccinomics approach for developing multi-epitope peptide pneumococcal vaccine, J. Biomol. Struct. Dyn. 37 (2019) 3524–3535, https://doi.org/10.1080/07391102.2018.1519460.

[45] I. Dimitrov, I. Bangov, D.R. Flower, I. Doytchinova, AllerTOP v.2–a server for in silico prediction of allergens, J. Mol. Model. 20 (2014) 2278, https://doi.org/10.1007/s00894-014-2278-5.

[46] M.R. Wilkins, E. Gasteiger, A. Bairoch, J.C. Sanchez, K.L. Williams, R.D. Appel, et al., Protein identification and analysis tools in the ExPASy server, Methods Mol. Biol. 112 (1999) 531–552, https://doi.org/10.1385/1-59259-584-7:531.

[47] C.N. Magnan, A. Randall, P. Baldi, SOLpro: accurate sequence-based prediction of protein solubility, Bioinformatics 25 (2009) 2200–2207, https://doi.org/10.1093/bioinformatics/btp386.

[48] J. Garnier, GOR secondary structure prediction method version IV, Meth Enzym, RF Doolittle Ed 266 (1998) 540–553.

[49] D.E. Kim, D. Chivian, D. Baker, Protein structure prediction and analysis using the Robetta server, Nucleic Acids Res. 32 (2004) W526–W531, https://doi.org/10.1093/nar/gkh468.

[50] M. Wiederstein, M.J. Sippl, ProSA-web: interactive web service for the recognition of errors in three-dimensional structures of proteins, Nucleic Acids Res. 35 (2007) W407–W410, https://doi.org/10.1093/nar/gkm290.

[51] K. Takeda, S. Akira, Toll-like receptors, Curr. Protoc. Im. 109 (2015), https://doi.org/10.1002/0471142735.im1412s109, 14.2.1-.2.0.

[52] K. Vijay, Toll-like receptors in immunity and inflammatory diseases: past, present, and future, Int Immunopharmacol 59 (2018) 391–412, https://doi.org/10.1016/j.intimp.2018.03.002.

[53] D. Kozakov, D.R. Hall, B. Xia, K.A. Porter, D. Padhorny, C. Yueh, et al., The ClusPro web server for protein-protein docking, Nat. Protoc. 12 (2017) 255–278, https://doi.org/10.1038/nprot.2016.169.

[54] G.C.P. van Zundert, J. Rodrigues, M. Trellet, C. Schmitz, P.L. Kastritis, E. Karaca, et al., The HADDOCK2.2 web server: user-friendly integrative modeling of biomolecular complexes, J. Mol. Biol. 428 (2016) 720–725, https://doi.org/10.1016/j.jmb.2015.09.014.

[55] R.A. Laskowski, J. Jabłońska, L. Pravda, R.S. Vařeková, J.M. Thornton, PDBsum: structural summaries of PDB entries, Protein Sci. 27 (2018) 129–134, https://doi.org/10.1002/pro.3289.

[56] C. Kutzner, S. Páll, M. Fechner, A. Esztermann, B.L. de Groot, H. Grubmüller, Best bang for your buck: GPU nodes for GROMACS biomolecular simulations, J. Comput. Chem. 36 (2015) 1990–2008, https://doi.org/10.1002/jcc.24030.

[57] J.A. Maier, C. Martinez, K. Kasavajhala, L. Wickstrom, K.E. Hauser, C. Simmerling, ff14SB: improving the accuracy of protein side chain and backbone parameters from ff99SB, J Chem Theory Comput 11 (2015) 3696–3713, https://doi.org/10.1021/acs.jctc.5b00255.

[58] H.J. Berendsen, Jv Postma, W.F. Van Gunsteren, A. DiNola, J.R. Haak, Molecular dynamics with coupling to an external bath, The Journal of chemical physics 81 (1984) 3684–3690, https://doi.org/10.1063/1.448118.

[59] M. Parrinello, A. Rahman, Strain fluctuations and elastic constants, J. Chem. Phys. 76 (1982) 2662–2666, https://doi.org/10.1063/1.443248.

[60] B. Hess, P-LINCS: a parallel linear constraint solver for molecular simulation, J Chem Theory Comput. 4 (2008) 116–122, https://doi.org/10.1021/ct700200b.

[61] T. Darden, D. York, L. Pedersen, Particle mesh Ewald: an N· log (N) method for Ewald sums in large systems, The Journal of chemical physics. 98 (1993) 10089–10092, https://doi.org/10.1063/1.464397.

[62] M.S. Valdés-Tresanco, M.E. Valdés-Tresanco, P.A. Valiente, E. Moreno, gmx_MMPBSA: a new tool to perform end-state free energy calculations with GROMACS, J. Chem. Theor. Comput. 17 (2021) 6281–6291, https://doi.org/10.1021/acs.jctc.1c00645.

[63] N. Rapin, O. Lund, M. Bernaschi, F. Castiglione, Computational immunology meets bioinformatics: the use of prediction tools for molecular binding in the simulation of the immune system, PLoS One 5 (2010) e9862, https://doi.org/10.1371/journal.pone.0009862.

[64] F. Zhu, C. Tan, C. Li, S. Ma, H. Wen, H. Yang, et al., Design of a multi-epitope vaccine against six Nocardia species based on reverse vaccinology combined with immunoinformatics, Front. Immunol. 14 (2023) 1100188, https://doi.org/10.3389/fimmu.2023.1100188.

[65] A. Grote, K. Hiller, M. Scheer, R. Münch, B. Nörtemann, D.C. Hempel, et al., JCat: a novel tool to adapt codon usage of a target gene to its potential expression host, Nucleic Acids Res. 33 (2005) W526–W531, https://doi.org/10.1093/nar/gki376.

[66] C.Y. Tseng, F. Murtada, L.Y.T. Chou, Precision nanoscale patterning of TLR ligands for improved cancer immunotherapy, Cell Rep Methods 4 (2024) 100782, https://doi.org/10.1016/j.crmeth.2024.100782.

[67] R.S. Andersen, A. Anand, D.S.L. Harwood, B.W. Kristensen, Tumor-associated microglia and macrophages in the glioblastoma microenvironment and their implications for therapy, Cancers 13 (2021), https://doi.org/10.3390/cancers13174255.

[68] M. Kwissa, S.P. Kasturi, B. Pulendran, The science of adjuvants, Expert Rev. Vaccines 6 (2007) 673–684, https://doi.org/10.1586/14760584.6.5.673.

[69] M. Tahir Ul Qamar, S. Ahmad, I. Fatima, F. Ahmad, F. Shahid, A. Naz, et al., Designing multi-epitope vaccine against Staphylococcus aureus by employing subtractive proteomics, reverse vaccinology and immuno-informatics approaches, Comput. Biol. Med. 132 (2021) 104389, https://doi.org/10.1016/j.compbiomed.2021.104389.
[70] V. Solanki, V. Tiwari, Subtractive proteomics to identify novel drug targets and reverse vaccinology for the development of chimeric vaccine against Acinetobacter baumannii, Sci. Rep. 8 (2018) 9044, https://doi.org/10.1038/s41598-018-26689-7.
[71] M. Hebditch, M.A. Carballo-Amador, S. Charonis, R. Curtis, J. Warwicker, Protein-Sol: a web tool for predicting protein solubility from sequence, Bioinformatics 33 (2017) 3098–3100, https://doi.org/10.1093/bioinformatics/btx345.
[72] D.D. Chaplin, Overview of the immune response, J. Allergy Clin. Immunol. 125 (2010) S3–S23, https://doi.org/10.1016/j.jaci.2009.12.980.
[73] E. Mahdevar, A. Kefayat, A. Safavi, A. Behnia, S.H. Hejazi, A. Javid, et al., Immunoprotective effect of an in silico designed multiepitope cancer vaccine with BORIS cancer-testis antigen target in a murine mammary carcinoma model, Sci. Rep. 11 (2021) 23121, https://doi.org/10.1038/s41598-021-01770-w.
[74] I.F. Pollack, R.I. Jakacki, L.H. Butterfield, R.L. Hamilton, A. Panigrahy, D.M. Potter, et al., Antigen-specific immune responses and clinical outcome after vaccination with glioma-associated antigen peptides and polyinosinic-polycytidylic acid stabilized by lysine and carboxymethylcellulose in children with newly diagnosed malignant brainstem and nonbrainstem gliomas, J. Clin. Oncol. 32 (2014) 2050–2058, https://doi.org/10.1200/jco.2013.54.0526.
[75] Z. Hu, D.E. Leet, R.L. Allesøe, G. Oliveira, S. Li, A.M. Luoma, et al., Personal neoantigen vaccines induce persistent memory T cell responses and epitope spreading in patients with melanoma, Nat Med 27 (2021) 515–525, https://doi.org/10.1038/s41591-020-01206-4.
[76] R.A. Fenstermaker, M.J. Ciesielski, J. Qiu, N. Yang, C.L. Frank, K.P. Lee, et al., Clinical study of a survivin long peptide vaccine (SurVaxM) in patients with recurrent malignant glioma, Cancer Immunol. Immunother. 65 (2016) 1339–1352, https://doi.org/10.1007/s00262-016-1890-x.